



Research Papers

Synthesis, optical band gap and thermoelectric properties of $\text{Sr}_{1+x}\text{TiS}_{3-y}$ chalcogenide perovskites

Jinan H. Al Shuhaib^{a,*}, Jose F. Fernández^{a,b}, Julio Bodega^a, José R. Ares^a, Isabel J. Ferrer^{a,b}, Fabrice Leardini^{a,b}

^a Departamento de Física de Materiales, Universidad Autónoma de Madrid, Campus de Cantoblanco, E-28049 Madrid, Spain

^b Instituto Nicolás Cabrera, Universidad Autónoma de Madrid, Campus de Cantoblanco, E-28049 Madrid, Spain

ARTICLE INFO

Keywords:

Chalcogenide perovskites
Strontium titanium sulfide
Solid-gas reaction
Band gap energy
Seebeck coefficient

ABSTRACT

Inorganic chalcogenide perovskites are semiconductors with attractive optoelectronic properties, which make them of interest in different fields, such as energy harvesting. Some of these compounds have been poorly investigated to date. For instance, very few works deal with the synthesis and characterization of $\text{Sr}_{1+x}\text{TiS}_3$. Here we present a novel synthesis procedure to obtain $\text{Sr}_{1+x}\text{TiS}_{3-y}$ powders. Moreover, we show for the first time an experimental characterization of some fundamental properties of this compound that may be relevant for many potential applications. First, we demonstrate that this perovskite shows very high thermal stability (up to 700°C in air and up to 1200°C in Ar atmosphere). Next, we experimentally determine its optical band gap (about 0.97 eV) corresponding to a direct allowed transition, in agreement with previous predictions. Finally, we demonstrate a tuneable Seebeck coefficient (changing from n-type to p-type behaviour) by changing the amount of sulfur vacancies.

1. Introduction

Chalcogenide perovskites have recently attracted significant attention due to their promising optoelectronic properties in the visible and infrared regions, with good thermal stability, composed of non-toxic and abundant elements. These unique properties make these materials good candidates for many applications, such as photonic, optoelectronic, and energy harvesting [1–3]. In particular, some recent theoretical works point out that these compounds can have good properties for thermoelectric applications and high thermal stability [4]. However, as far as our knowledge goes, no experimental data have been reported to date regarding the thermoelectric properties of this class of materials.

Chalcogenide perovskites have the general formula ABX_3 , with A being a group II cation (i.e., Ca^{2+} , Sr^{2+} , or Ba^{2+}), B a group IV transition metal (i.e., Ti^{4+} , Zr^{4+} , or Hf^{4+}), and X a chalcogen anion (S^{2-} or Se^{2-}) [5–7]. Here we will focus on a specific chalcogenide perovskite, SrTiS_3 , which has not been widely studied until now [6,8].

Several groups have prepared this compound before by following different reaction routes. The first paper was reported by V. Hahn et al. [9], who used a reaction between SrS and TiS_2 powders at high temperatures. Next, B. Okai, et al. [10] prepared $\text{Sr}(\text{Ti}_{1-x}\text{Zr}_x)\text{S}_3$ by

sulfurization of the corresponding oxides using a flow of CS_2 . The reaction was achieved at temperatures ranging from 800°C to 1000°C. M. Saeki and M. Onoda used a similar procedure [11] to obtain Sr_xTiS_3 ($x=1.05\text{--}1.22$). On the other hand, O. Gourdon et al. [12] obtained $\text{Sr}_{9/8}\text{TiS}_3$ single crystals from a mixture of the pure elements ($\text{Sr}:\text{Ti}:\text{S} = 1.2:1:3$). Finally, SrTiS_3 single crystals were synthesized by using SrS , Ti and S powders through a chemical vapour transport method with iodine as a transport agent [8].

In this manuscript, we present original results on the synthesis of SrTiS_3 (STS hereafter) using a novel procedure. We prepared STS powders by sulfurization of SrTiO_3 (STO hereafter) with CS_2 . This is the same reaction previously carried out by other researchers [10,11]. However, in those works, the reaction occurred in open quartz reactors by flowing Ar/CS_2 mixtures, whereas in the present work we used sealed evacuated quartz ampoules containing the oxide and CS_2 , therefore in absence of any inert gas. Our method enables the utilization of a reduced quantity of CS_2 precursor compared to the open reactor operated under CS_2 flow.

Structural properties and chemical composition of the samples have been characterized by x-ray Powder Diffraction, Raman spectroscopy and energy dispersive X-ray analysis (EDX). The optical band gap of STS has been investigated by diffuse reflectance spectroscopy of the obtained

* Corresponding author.

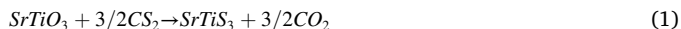
E-mail address: jinan.awadh@estudiante.uam.es (J.H.A. Shuhaib).

powders pressed in pellets. Thermal stability studies have been done in air and in Ar atmospheres, showing that STS presents a very high stability. Finally, Seebeck coefficient measurements allow us to characterize the thermoelectric properties of STS for the first time.

2. Experimental details

2.1. Synthesis methods

Chalcogenide perovskites with nominal composition SrTiS_3 have been synthesized by solid-gas reaction in sealed evacuated quartz ampoules at temperatures ranging from 800°C to 1050°C. To this aim, we followed the sulfurization of the corresponding perovskite oxide SrTiO_3 with CS_2 as a chalcogen precursor, according to the reaction:



STO powders (Sigma-Aldrich 99.9%) and CS_2 (1.02214 EMSUR) starting materials were stored in the air. Some attempts were also done using elemental sulfur as a chalcogen source (138338-Merck). The reactions were done in sealed quartz ampoules of 10 mm in diameter, 170 mm in length and 2.5 mm wall thickness. The ampoules were cleaned by oxygen plasma (Diener, model Zepto). The ideal gas equation was used to calculate the amount of CS_2 (or S) necessary to have a maximum pressure of 10 bar inside the ampoules when heating at high temperatures. Then, we calculated the corresponding masses of the oxide precursor in order to ensure an excess of CS_2 (or gaseous S_2) in the ampoules (with a minimum pressure of 3 bar if all the oxides reacted to form the corresponding sulfides). The excess of CS_2 (or S) was condensed in the cold side of the ampoules during their cooling down.

The oxide precursor was placed at the bottom of the quartz ampoule, and then we added CS_2 with a Pasteur pipette. All these handlings were made under Ar atmosphere (using a glove box JACOMEX, Model Campus, and a glove bag) to avoid contamination with oxygen or moisture inside the ampoules. Then we closed the Ar-filled quartz ampoule with a metallic valve using Viton fittings and connected it to a diffusion pump to fuse it by using a blowtorch and seal it under a residual vacuum in the 10^{-6} mbar range. The bottom of the ampoule, where the oxide precursor and CS_2 were placed, was immersed in a Dewar filled with liquid nitrogen to avoid the sublimation of CS_2 during sealing in a vacuum. Then a thermocouple (R-type) was attached to the ampoule to monitor the sulfurization temperature. Ampoules were heated up by using a tube furnace (Carbolite). A scheme of the experimental system is shown in the Supporting Information (Fig. S1). The sulfurization time was seven days for all samples. Samples were cooled down naturally by switching off the furnace. At room temperature, ampoules were broken in a ventilated hood (due to an excess of CS_2), and the obtained samples were ground in an agate mortar to obtain homogenous powders. All samples were stored and handled in an ambient atmosphere.

2.2. Materials characterizations

2.2.1. X-ray powder diffraction

Structural properties have been analysed by X-ray Powder Diffraction (XRPD) measurements in a Bruker D8 diffractometer. Diffraction patterns were recorded using a θ -2 θ configuration with a step of 0.02° and an integration time of 2 s. $\text{Cu K}\alpha_1$ radiation with $\lambda = 1.5406 \text{ \AA}$ and power settings of 45 kV and 40 mA have been used. Rietveld refinement analyses have been done using Fullprof Suite software on scans from 10° to 80°.

2.2.2. Chemical and morphological characterizations

Energy dispersive X-ray analyses (EDX) have been acquired with a Quantax system coupled to a scanning electron microscope (SEM) Hitachi S3000 model. EDX spectra and SEM images were acquired with 15 kV accelerating voltage and a working distance of 15 mm. Different

magnifications ranging from 100X to 6000X were used.

2.2.3. Raman spectroscopy

The prepared samples have been characterized by Raman spectroscopy at room temperature in a Witec ALPHA 300AR instrument using a confocal microscope with a 100X objective. A green laser with an excitation wavelength of 532.3 nm and a power of 0.2 mW has been used.

2.2.4. Optical band gap

Diffuse reflectance spectroscopy measurements have been done in a Perkin Elmer Lambda 950 UV-vis spectrometer. Spectra were recorded in the 300–2000 nm range. We prepared pellets of 5 mm in diameter and about 1 mm in thickness by pressing the powders in a dye under 0.75 GPa.

2.2.5. Thermal stability

Thermal stability characterizations were performed both under dry air and under Ar atmospheres. Differential scanning calorimetry (DSC) and thermogravimetric analysis (TGA) measurements were simultaneously done on a SDT Q600-TA. Instrument. Concomitant gas analyses were done by coupling a mass spectrometer Thermostat GSD 301 T3. These measurements allowed us to identify evolved or consumed molecules as a function of the temperature. Samples were heated in alumina crucibles, from 25°C to 1200°C at a constant heating rate of 10°C/min.

2.2.6. Thermoelectric measurements

The Seebeck coefficient of STS pellets has been measured with a homemade experimental setup (see Fig. S2) [13]. A pair of aluminium blocks with embedded heaters act as thermal reservoirs allowing varying the average temperature (T) and the temperature difference along the sample (ΔT). The sample was placed between both blocks. Then, two electrical contacts were made using carbon conductive paint between the two separated positions in the pellet and two iron sheets to record the thermoelectric voltage as a function of the temperature gradient. The thermoelectric voltage (ΔV) is monitored with two voltage probes placed on the iron sheets. ΔT is measured by two thermocouples placed on the iron sheets close to the electric contact with the pellets. The Seebeck coefficient can be determined as the linear ΔV vs ΔT plot slope. Telkes criterium [14] was chosen about the sign of the Seebeck coefficient, i.e., positive for p-type and negative for n-type conduction. The resistivity of STS pellets has been measured making mechanical contacts on them with two metallic probes and using a Keithley 2000 multimeter.

3. Results and discussion

3.1. Chemical composition, structural properties, and thermal stability

We first investigated the sulfurization of STO using elemental sulfur as a chalcogen source (see Table S1 in the S.I.). However, we observed that no reaction took place between STO and elemental S after seven days at 900°C. The colour of the STO powder remained the same after the treatment, and the XRPD pattern of the obtained powder indicates that it was STO (See Fig. S3 in the S.I.). The use of CS_2 as a chalcogen source for STO sulfurization was then investigated using the same growth conditions (900°C for seven days). Our results demonstrate that CS_2 is much more reactive with the oxide than elemental sulfur, which may be due to the formation of CO_2 as a reaction by-product that may favour the reaction thermodynamics owing to its high stability.

A clear change in the colour of the powder was observed after sulfurization, passing from white to black (see Fig. 1a and b). Moreover, an increase in the mass of this powder of about 20 % was observed after sulfurization. This mass increase is close to that predicted according to reaction (1), namely, 26 %. The difference between the observed mass increase and the calculated one is ascribed to the loss of some quantities of the solid powders during their collection from the quartz

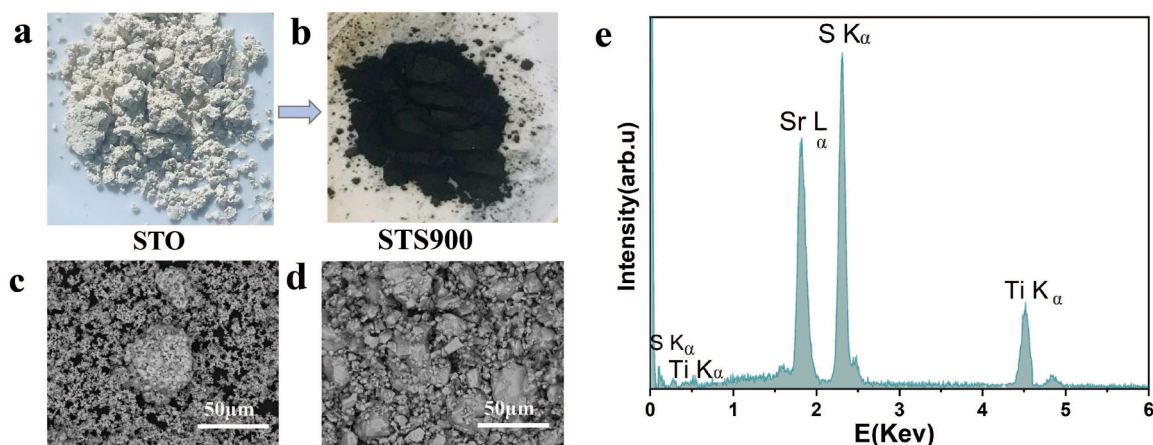


Fig. 1. Optical images of (a) STO (white) and (b) STS (black) powders. SEM images of (c) STO and (d) STS. (e) Typical EDX spectrum of STS sample.

ampoule, as well as to deviations in the stoichiometry of the obtained chalcogenide perovskite. The chemical composition of the obtained sample was determined by EDX by measuring different particles of the same powder to account for possible inhomogeneities and determine the uncertainty associated with each elemental abundance. The typical EDX spectrum of STS is shown in Fig. 1e. Only Sr, Ti and S were detected in all the analysed particles. A stoichiometry of $\text{Sr}_{1.04(4)}\text{Ti}_{2.75(8)}\text{S}$ has been obtained. These values are close to the stoichiometric 1:1:3 atomic ratios. However, some sulfur deficiency is present which, is usually observed in similar chalcogenide perovskites such as SrTiS_3 [8] and BaZrS_3 [6,15]. Moreover, strontium over-stoichiometry has also been reported in SrTiS_3 [12,16].

The crystalline structure of the STS sample has been investigated by XRPD measurements. Diffraction patterns of the starting STO powder and the STS sample obtained at 900°C, are shown in Fig. 2a. The diffraction pattern of STO corresponds to that reported in JCPDS 01-079-0174 file (space group pm-3m 221). An evident change in the diffraction pattern of STO after sulfurization is observed. The diffraction pattern of STS powders can be indexed with a single crystalline phase belonging to the trigonal R-3c space group (S.G. 167). The observation of that crystalline phase agrees with the results published by Gourdon

et al. with samples of similar composition [12].

Rietveld refinements of the diffraction patterns have been done to obtain the lattice parameters and the unit cell volume of the STS sample, as shown in Fig. S4 at S.I. Different models have been used for these refinements, according to previously published results: trigonal R-3c space group (S.G. 167) [12] and trigonal P-3 space group (S.G. 147) [16]. The best results have been obtained with the S.G. 167 structure. For the refinement, the occupation of Sr, Ti and S sites have been fixed, considering 54 atoms of Sr, 48 atoms of Ti and 144 atoms of S per unit cell. However, it must be noticed that according to previous works [11, 17], SrTiS_3 crystallize in an incommensurate structure where the TiS_3 units and the Sr units share the same a parameter but have different c parameters, $c\text{TiS}_3$ and $c\text{Sr}$, that are incommensurate. To fit the data properly, a super-space group formalism must be used [8,12,16]. The incommensurate character of the structure is reflected in the large chi-square parameters obtained from the refinement done here. Some of the smaller diffraction peaks are not well fitted by the model used by us. Provided that the peak positions are adequately replicated with the model employed here, it is possible to obtain lattice parameters with high accuracy. The lattice parameters are presented in Table S2 of the Supporting Information.

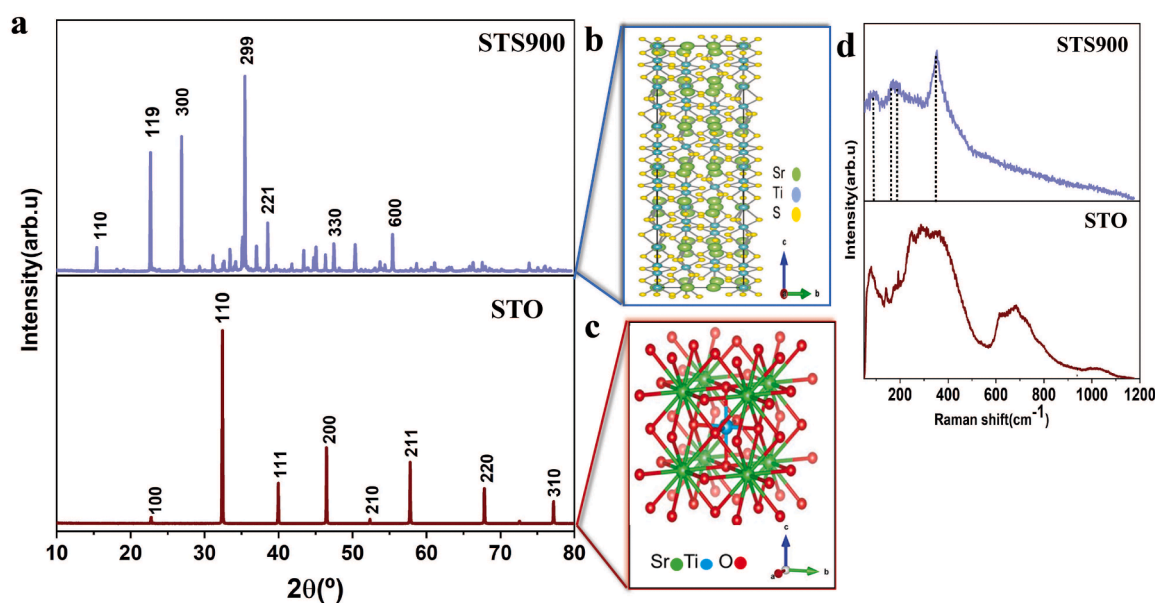


Fig. 2. (a) Diffraction patterns of the starting STO oxide and STS chalcogenide. Miller indexes of the main diffraction peaks are indicated. Schematic crystal structures of (b) STS (side view along a axis) and (c) STO (side view along a axis). (d) Raman spectra of the starting STO oxide and STS chalcogenide.

The structural properties of the samples have been also characterized by Raman spectroscopy. The starting STO material shows the typical Raman bands characteristic of this compound [18], as it can be seen in Fig. 2d. The typical spectrum of STS is also shown in Fig. 2d. Raman spectra recorded at different particles are reproducible, indicating that the STS sample is homogeneous and presents a single crystalline phase, in good agreement with XRPD results. STS presents four broad Raman bands at ~ 115 , 185, 210 and 370 cm^{-1} . This Raman spectrum is similar to that reported for SrTiS_3 single crystals [8].

The thermal stability of STS in dry air has been investigated by TGA and DSC measurements. Concomitant Mass Spectrometry measurements were done to analyse the composition of the gases released and consumed during the TGA-DSC runs. The TGA and DSC signals recorded during the heating of the sample can be seen in Fig. 3a. There is an initial mass loss of about 2.4 wt.% below 250°C . Mass spectrometry measurements reveal the release of H_2O and CS_2 species in this temperature interval (see Fig. S5 in the Supporting Information). Therefore, we can relate this initial mass loss to the elimination of H_2O and CS_2 residues adsorbed in the samples.

The samples are stable up to about 700°C , with minimal mass loss lower than 1 wt.%. Then, a significant mass loss is observed, along with a decrease in the ionic signal at $m/q=32$, related to the consumption of O_2 present in the air flow (Fig. 3b). At the same time, there is an increase in the ionic signals at m/q values equal to 48 (not shown) and 64 (Fig. 3c). The relative intensities of these ionic fragments indicate that SO_2 molecules are released from the samples. Therefore, we can relate the observed mass loss to the following oxidation reaction:



The reaction is stopped at around 750°C , where a mass increase starts (Fig. 3a), along with the recovery of the O_2 background signal (Fig. 3b). This can be related to the formation of strontium carbonate by the reaction of the SrTiO_3 shell produced by reaction (2) and CO_2 traces present in the air flow, according to the following reaction:



That carbonate is afterwards decomposed at higher temperatures, by following the reverse of the reaction (3) and giving rise to the release of CO_2 , as evidenced by the ionic signal at $m/q=44$ (see Fig. 3c). Finally, a second release of SO_2 is observed, along with a mass decrease above 950°C . This can be ascribed to the oxidation of the remaining SrTiS_3

phase present at the core of the powder particles following the reaction (2). The XRPD characterization of the product obtained after the TGA-DSC run in the air reveals that it is SrTiO_3 (see Fig. S6 in the S.I.). This picture is also in agreement with the total mass loss observed of 21 wt.%, which is close to the estimated mass loss of the sample (considering its chemical composition determined by EDX), which is equal to 23 wt.%. SrTiS_3 shows higher thermal stability than other perovskite sulfides, such as BaZrS_3 , which are thermally stable in the air until 500°C [19].

The thermal stability of STS samples under Ar atmosphere has also been investigated by DSC and TGA. Samples heated in Ar present an initial mass loss below 200°C (see Fig. S7 in the S.I.). This mass loss is like that observed under dry air, and therefore it is ascribed to the release of H_2O and CS_2 traces present in the samples. When heated at higher temperatures, there is a slight gradual mass loss of about 5 wt.% until 1200°C . This reveals the extremely high thermal stability of the SrTiS_3 phase.

3.2. Optical band gap and thermoelectric properties

The optical properties of STS powders have been investigated by diffuse reflectance spectroscopy. It can be seen that the diffuse reflectance decreases below 3 % for wavelengths lower than about 1300 nm (see Fig. 4a), indicating a strong optical absorption in the near IR and visible regions. The Kubelka-Munk function [20] has been used (since it is proportional to the absorption coefficient) to determine the optical band gap energy by using a Tauc plot (Fig. 4b), considering a direct allowed transition. Additional details about the use of the Kubelka-Munk methodology can be found at the S.I. (see Fig. S8). The obtained band gap of STS is equal to 0.97 eV. This value is close to that theoretically predicted in previous reports [7,15]. In particular, reference [7] reported a direct band gap (ranging from $\sim 0.2\text{ eV}$ to $\sim 0.9\text{ eV}$ depending on the crystal structure) at the Brillouin centre based on theoretical calculations for this compound. It is worth to mention that, as far as we know, this is the first experimental determination of the optical band gap in STS.

The semiconducting nature of the STS phase, evidenced by the optical characterizations, suggests that this material can be of interest for applications related to its transport properties. Therefore, we measured the room temperature thermoelectric properties of STS. Fig. 4c shows the variation of the thermoelectric voltage (ΔV) as a function of the temperature difference (ΔT). A Seebeck coefficient of $-385\text{ }\mu\text{V/K}$ has been determined from the slope of this plot. This value indicates an n-type character of the STS sample. This result and the extremely high thermal stability of this compound imply that this material has promising properties for its use in thermoelectric applications.

3.3. Influence of the growth temperature on chemical, structural and thermoelectric properties

After the successful synthesis of STS, we focused on investigating the influence of growth temperature on its properties ($800^\circ\text{C} < T < 1050^\circ\text{C}$). The growth conditions are shown in Table S1 at S.I.

From an experimental point of view, using a temperature as low as possible should be desirable. Therefore, we repeated the synthesis using a growth temperature of 800°C . Chemical analyses of the samples have been done by EDX to obtain elemental abundances. A black powder was obtained having a lower sulfur content than the samples prepared at higher temperatures (see table S1 at S.I.). However, that sample presented a complex diffraction pattern showing many peaks (see Fig. S9 in the S.I.), and we have not resolved the corresponding crystal structure. A complex diffraction pattern has been reported before when trying the synthesis of STS in the same temperature range using a different reaction route [9].

On the other hand, when increasing the growth temperature from 900 to 1050°C , the obtained powders present a similar XRPD pattern to

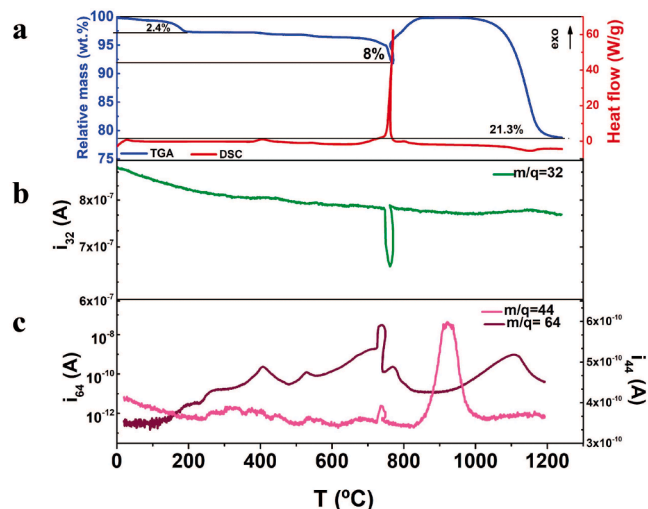


Fig. 3. (a) TGA (blue line) and DSC (red line) traces for STS recorded in dry air atmosphere; (b) mass spectrometric ionic current recorded at $m/q=32$ (corresponding to O_2 specie); (c) mass spectrometric ionic currents recorded at $m/q=64$ (corresponding to SO_2 specie) and at $m/q=44$ (corresponding to CO_2 specie).

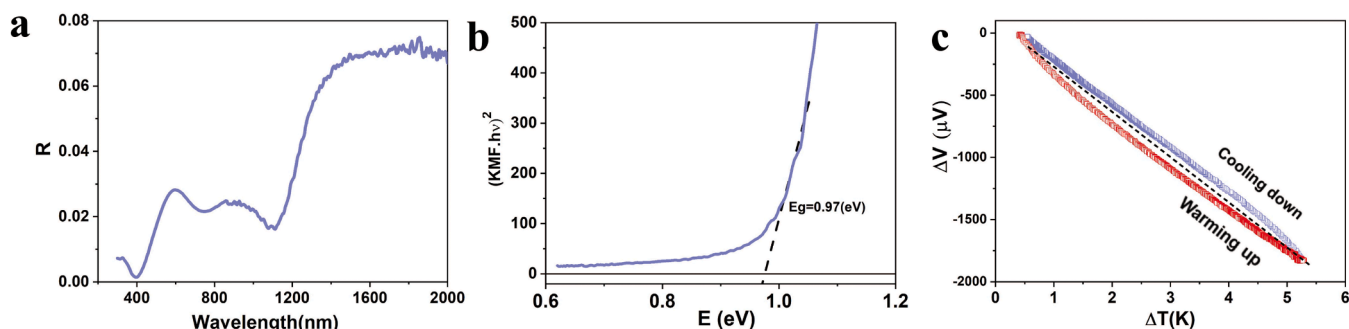


Fig. 4. (a) Diffuse reflectance spectrum of STS. (b) Tauc plot obtained with the Kubelka-Munk function (KMF) considering a direct allowed transition. The dashed line is the linear fit to obtain the band gap energy. (c) Thermoelectric voltage (ΔV) as a function of the temperature difference (ΔT) along the STS pellets recorded during a warming up and cooling down cycle. The Seebeck coefficient can be extracted from the slope of this plot.

that at 900°C, which can be indexed with the same space group (S.G. 167). Rietveld refinements of XRPD patterns have also been done for all samples (see Figs. S10-S12 at the S.I.).

Lattice parameters obtained are listed in Table S2 at S.I. The evolution of the elemental abundance ratios (S/M, being M=Ti, Sr, and Ti+Sr) as a function of the growth temperature is shown in Fig. 5a. It is interesting to realize that there is a correlation between the unit cell volume determined by XRPD refinements and the S/(Sr+Ti) ratio measured by EDX, as shown in Fig. 5b. This indicates that the presence of sulfur vacancies shrinks the unit cell. In addition, the peak positions and full width at half maximum (FWHM) of the principal Raman band also changes with the S/(Sr+Ti) ratio, as it can be seen in Fig. 5c.

As it concerns the optical band gap determined from diffuse reflectance measurements, obtained values lie in the range from 0.94–0.97 eV for all samples, thus implying that the growth temperature does not affect the optical properties of the samples. However, the observed changes in elemental abundances have a strong effect on the Seebeck coefficient (see Fig. 6a). Seebeck coefficient values correlate with the sulfur vacancies content (i.e., y values) in the samples, as shown in Fig. 6b. Samples with a lower sulfur vacancy content present a negative Seebeck coefficient (n-type behaviour). When increasing the amount of sulfur vacancies, the Seebeck coefficient increases, shifting to positive values (p-type behaviour). A similar effect has been observed with the parent perovskite SrTiO_{3-y} where a shift towards positive values was observed by increasing the amount of oxygen vacancies [21].

Finally, we determined the power factor ($\text{PF} = S^2/\rho$), where S is the Seebeck coefficient and ρ is the electrical resistivity. The obtained ρ values were in the range of 85–240 $\Omega\cdot\text{m}$, being higher for the p-type sample than for the n-type ones. With these values the estimated power factors lie in the range $4\cdot 10^{-9}$ $\text{mW m}^{-1} \text{K}^{-2}$ and $6\cdot 10^{-7}$ $\text{mW m}^{-1} \text{K}^{-2}$. As far as we know, no experimental nor theoretical values of thermoelectric properties of STS have been reported so far. However, there are few theoretical studies of some properties (Seebeck coefficient, thermal

conductivity, power factor and ZT values) for other perovskite chalcogenides [4,22–25]. For instance, the reported theoretical PF value for BaZrS_3 is $5\cdot 10^{-3}$ $\text{mW m}^{-1} \text{K}^{-2}$ [25].

4. Conclusions

A novel approach for the growth of single-phase $\text{Sr}_{x+1}\text{TiS}_{3-y}$ chalcogenide perovskite has been used by solid-gas reaction of SrTiO_3 powders with CS_2 in sealed quartz ampoules at high temperatures. Crystal structure and chemical composition have been characterized by X-ray diffraction and EDX, respectively. The thermal stability of the obtained perovskites has been investigated here for the first time. An extremely high thermal stability has been observed (up to 700°C in dry air and up to 1200°C in Ar atmosphere).

The optical properties have also been experimentally measured for the first time by diffuse reflectance measurements in the UV-vis-NIR range showing a strong absorption in the visible region. A direct allowed transition with a band gap energy value in the 0.94–0.97 eV range, has been obtained. Moreover, the transport properties have been characterized based on Seebeck coefficient measurements. A strong dependence of the Seebeck coefficient on the chemical composition has been found. In turn, chemical composition, in particular the sulfur to metal ratio (S/M), can be tuned by varying the growth temperature. A change from n-type to p-type behaviour has been observed by increasing the sulfur vacancies content. The characteristics of the obtained chalcogenide perovskite SrTiS_3 will open new opportunities for designing novel devices for renewable energy applications.

Author contributions

Jinan H. Al Shuhaib participated in all the tasks, including the synthesis and characterization of the samples. Jose F. Fernández and Julio Bodega made the XRPD analysis and Rietveld refinements. Isabel J.

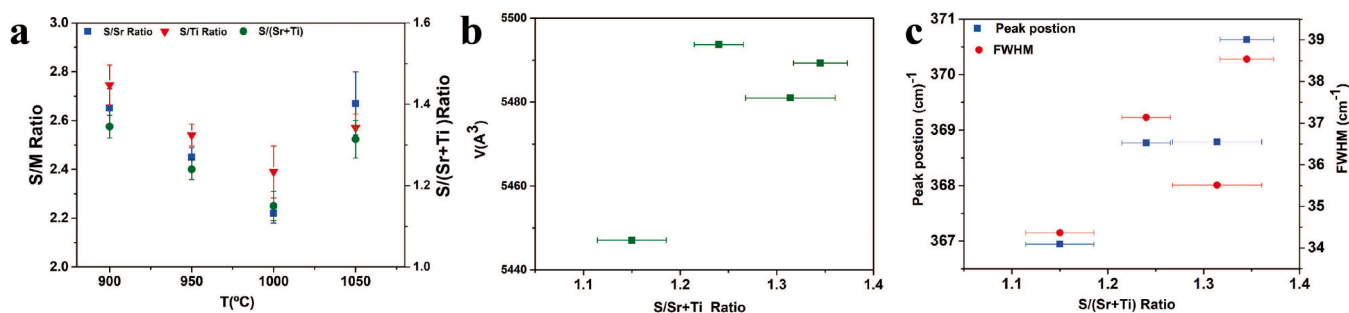


Fig. 5. (a) S/Sr, S/Ti and S/(Sr+Ti) atomic ratios for STS samples as a function of the sulfurization temperature. (b) Correlation between the unit cell volume obtained by Rietveld refinement of the XRPD patterns and the S/(Sr+Ti) ratio determined by EDX. (c) Peak position and FWHM for the most prominent Raman peak (at 370 cm^{-1}) as a function of the S/(Sr+Ti) in the samples determined by EDX.

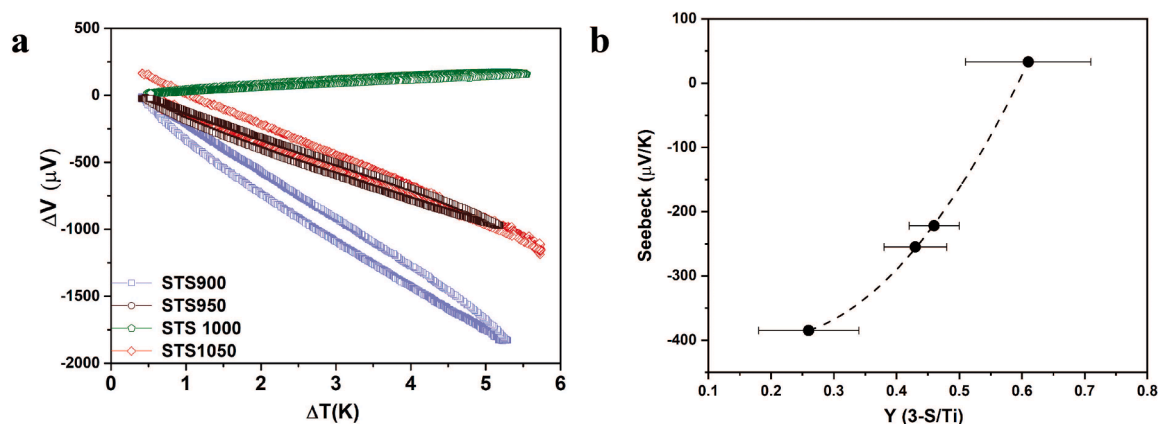


Fig. 6. (a) Thermoelectric voltage (ΔV) as a function of the temperature difference (ΔT) along the STS pellets recorded during a warming up and cooling down cycle. (b) Seebeck coefficient as a function of the sulfur vacancies content in the samples. The dashed line is a guide for the eye.

Ferrer and Jose R. Ares made the Seebeck coefficient measurements. Fabrice Leardini conceived the synthesis of the samples and participated in that task, and he also participated in the thermal stability characterization and the optical measurements. All authors have contributed to the discussion of the obtained data and the writing of the manuscript.

Declaration of Competing Interest

The authors declare that they have no known competing financial interests or personal relationships that could have appeared to influence the work reported in this paper.

Data availability

Data will be made available on request.

Acknowledgements

The authors acknowledge the technical assistance of Mr F. Moreno, and the use of SIDI and Segainvex facilities at Universidad Autónoma de Madrid. This research has been funded by Spanish MICINN under RTI2018-099794-B-I00 grant.

Supplementary materials

Supplementary material associated with this article can be found, in the online version, at [doi:10.1016/j.materresbull.2023.112405](https://doi.org/10.1016/j.materresbull.2023.112405).

References

- [1] S. Niu, H. Huan, Y. Liu, M. Yeung, K. Ye, L. Blankemeier, Th. Orvis, D. Sarkar, D. Singh, R. Kapadia, J. Ravichandran, Bandgap control via structural and chemical tuning of transition metal perovskite chalcogenides, *Adv. Mater.* 29 (2017), 1604733, <https://doi.org/10.1002/adma.201604733>.
- [2] J. Cuya, N. Sato, K. Yamamoto, H. Takahashi, A. Muramatsu, Thermogravimetric study of the sulfurization of $SrTiO_3$ nanoparticles using CS_2 , *Thermochimica Acta* 419 (2004) 215–221, <https://doi.org/10.1016/j.tca.2004.01.033>.
- [3] S. Niu, B. Zhao, K. Ye, E. Bianco, J. Zhou, M. McConney, Ch. Settens, R. Haiges, R. Jaramillo, J. Ravichandran, Crystal growth and structural analysis of perovskite chalcogenide $BaZrS_3$ and Ruddlesden–Popper phase $Ba_3Zr_2S_7$, *J. Mater. Res.* 34 (2019) 3819–3826, <https://doi.org/10.1557/jmr.2019.348>.
- [4] H. Shahmohamadi, S. Naghavi, Sulfide perovskites for thermoelectricity, *ACS Appl. Mater. Interface* 13 (2021) 14189–14197, <https://doi.org/10.1021/acsami.0c22842>.
- [5] J. Márquez, M. Rusu, H. Hempel, I. Ahmet, M. Kölbach, I. Simsek, L. Choubrac, G. Gurieva, R. Gunder, S. Schorr, Th. Unold, $BaZrS_3$ chalcogenide perovskite thin films by H_2S sulfurization of oxide, *J. Phys. Chem. Lett.* 12 (2021) 2148–2153, <https://doi.org/10.1021/acs.jpclett.1c00177>.
- [6] X. Wei, H. Hui a, Ch. Zhao, Ch. Deng, M. Han, Z. Yu, A. Sheng, P. Roy, A. Chen, J. Lin, D. Watson, Y. Yang, Realization of $BaZrS_3$ chalcogenide perovskite thin films for optoelectronics, *Nano Energy* 68 (2020), 104317, <https://doi.org/10.1016/j.nanoen.2019.104317>.
- [7] Y. Sun, M. Agiorgousis, P. Zhang, Sh. Zhang, Chalcogenide perovskites for photovoltaics, *Nano Lett.* 15 (2015) 581–585, <https://doi.org/10.1021/nl504046x>.
- [8] Sh. Niu, H. Zhao, Y. Zhou, H. Huan, B. Zhao, J. Wu, S. Cronin, H. Wang, J. Ravichandran, Mid-wave and long-wave infrared linear dichroism in a hexagonal perovskite chalcogenide, *Chem. Mater.* 30 (2018) 4897–4901, <https://doi.org/10.1021/acs.chemmater.8b02279>.
- [9] V. Hahn, U. Mutschke, Untersuchungen über ternäre Chalkogenide. XI. Versuche zur Darstellung von Thioperowskiten, *J. inorgan. General Chem. ZAAC* 288 (1957) 269–278, <https://doi.org/10.1002/zaac.19572880505>.
- [10] B. Okai, K. Takahashi, M. Saeki, J. Yoshimoto, Preparation and crystal structural of some complex sulphides at high pressure, *M. Res. Bulletin* 23 (1988) 1575–1584, [https://doi.org/10.1016/0025-5408\(88\)90245-0](https://doi.org/10.1016/0025-5408(88)90245-0).
- [11] M. Saeki, M. Onoda, Preparation of a new strontium titanium sulfide Sr_xTiS_3 ($x=1.05$ – 1.22) with infinity adaptive structure, *J. Solid State Chem.* 102 (1993) 100–105, <https://doi.org/10.1006/jssc.1993.1011>.
- [12] O. Gourdon, V. Petricek, M. Evain, A new structure type in the hexagonal perovskite family: structure determination of the modulated misfit compound $Sr_{9/8}TiS_3$, *Acta Cryst. B56* (2000) 409–418, <https://doi.org/10.1107/S0108768100002160>.
- [13] E. Flores, J. Ares, A. Gomez, M. Barawi, I. Ferrer, C. Sánchez, Thermoelectric power of bulk black-phosphorus, *Appl. Phys. Lett.* 106 (2015), 022102, <https://doi.org/10.1063/1.4905636>.
- [14] M. Telkes, Thermoelectric power and electrical resistivity of minerals, *Am. Mineral.* 35 (1950) 536–555.
- [15] S. Pereraa, H. Huia, Ch. Zhaoa, H. Xuea, F. Suna, Ch. Dengc, N. Grossa, Ch. Millevilled, X. Xuc, D. Watsond, B. Weinsteina, Y. Sune, Sh. Zhange, H. Zeng, chalcogenide perovskites – an emerging class of ionic semiconductors, *Nano energy* 22 (2016) 129–135, <https://doi.org/10.1016/j.nanoen.2016.02.020>.
- [16] O. Gourdon, L. Cario, V. Petricek, M. Evain, Synthesis, structure determination, and twinning of two new composite compounds in the hexagonal perovskite-like sulfide family: $Eu_{8/7}TiS_3$ and $Sr_{8/7}TiS_3$, *Z. Kristallogr.* 216 (2001) 541–555, <https://doi.org/10.1524/zkri.216.10.541.20366>.
- [17] M. Onoda, M. Saeki, A. Yamamoto, K. Kato, Structure refinement of the incommensurate composite crystal $Sr_{1.145}TiS_3$ through the Rietveld analysis process, *Acta Cryst. Sect. B49* (1993) 929–936, <https://doi.org/10.1107/S0108768193005324>.
- [18] Sh. Li, Y. Jia, Y. Yao, J. Yan, Sh. Xie, Raman spectra of $SrTiO_3$ prepared by direct current arc discharge plasma process, *Adv. Mater. Res.* 1004–1005 (2014) 415–419, <https://doi.org/10.4028/www.scientific.net/AMR.1004-1005.415>.
- [19] Sh. Niu, J. Guerrero, Y. Zhou, K. Ye, B. Zhao, B. Melot, J. Ravichandran, Thermal stability study of transition metal perovskite sulfides, *J. Mater. Res.* 33 (2018) 4135–4143, <https://doi.org/10.1557/jmr.2018.419>.
- [20] G. Kortum, W. Braun, D. Chem, G. Herzog, Principles and techniques of diffuse-reflectance spectroscopy, *Angew. Chem. Internat. Edit.* 2 (1963) 333–341, <https://doi.org/10.1002/anie.196303331>.
- [21] X. Feng, Y. Fan, N. Nomura, K. Kikuchi, L. Wang, W. Jiang, A. Kawasaki, Graphene promoted oxygen vacancies in perovskite for enhanced thermoelectric properties, *Carbon* 112 (2017) 169–176, <https://doi.org/10.1016/j.carbon.2016.11.012>.
- [22] X. Song, X. Shai, Sh. Deng, J. Wang, J. Li, X. Ma, X. Li, T. Wei, W. Ren, L. Gao, Y. Fu, H. Wang, Ch. Zeng, Anisotropic chalcogenide perovskite $CaZrS_3$: a promising thermoelectric material, *J. Phys. Chem. C* 126 (2022) 11751–11760, <https://doi.org/10.1021/acs.jpcc.2c02286>.

- [23] E. Agyemang, Ch. Adu, G. Balasubramanian, Ultralow lattice thermal conductivity of chalcogenide perovskite CaZrSe_3 contributes to high thermoelectric figure of merit, *Comput. Mater.* 5 (2019) 116, <https://doi.org/10.1038/s41524-019-0253-5>.
- [24] E. Agyemang, G. Balasubramanian, Understanding the extremely poor lattice thermal transport in chalcogenide perovskite BaZrS_3 , *ACS Appl. Energy Mater.* 3 (2020) 1139–1144, <https://doi.org/10.1021/acsaem.9b02185>.
- [25] E. Agyemang, N. Koratkar, G. Balasubramanian, Examining the electron transport in chalcogenide perovskite BaZrS_3 , *J. Mater. Chem. C* 9 (2021) 3892–3900, <https://doi.org/10.1039/D1TC00374G>.